PCCP

Accepted Manuscript

This is an *Accepted Manuscript*, which has been through the Royal Society of Chemistry peer review process and has been accepted for publication.

Accepted Manuscripts are published online shortly after acceptance, before technical editing, formatting and proof reading. Using this free service, authors can make their results available to the community, in citable form, before we publish the edited article. We will replace this *Accepted Manuscript* with the edited and formatted *Advance Article* as soon as it is available.

You can find more information about *Accepted Manuscripts* in the **Information for Authors**.

Please note that technical editing may introduce minor changes to the text and/or graphics, which may alter content. The journal's standard **Terms & Conditions** and the **Ethical guidelines** still apply. In no event shall the Royal Society of Chemistry be held responsible for any errors or omissions in this *Accepted Manuscript* or any consequences arising from the use of any information it contains.

Photophysics of Auramine-O: Electronic Structure Calculations and Nonadiabatic Dynamics Simulations†

Bin-Bin Xie, Shu-Hua Xia, Xue-Ping Chang, and Ganglong Cui[a]

Diphenylmethane dyes are very useful photoinduced molecular rotors; however, their photophysical mechanisms are still elusive until now. In this work, we adopted combined static electronic structure calculations (MS-CASPT2//CASSCF) and trajectory-based surface-hopping dynamics simulations (OM2/MRCI) to study the S_1 excited-state relaxation mechanism of a representative diphenylmethane dye Auramine-O. On the basis of the optimized S_1 minima and the computed emission bands, we have for the first time assigned experimentally proposed three transient states (i.e. S1-LE, S1-I1 or S1-I2, and S1-II). Mechanistically, upon irradiation to the S_1 state, the system first relaxes to the locally excited S_1 minimum (S1-LE). Starting from this point, there exist two kinds of relaxation paths to S1-II. In the sequential path, the system first evolves into S1-I1 or S1-I2 and then runs into S1-II; in the concerted one, the system, bypassing S1-I1 and S1-I2, directly runs into S1-II. In addition, the system can decay to the S_0 state in the vicinity of three S_1/S_0 conical intersections i.e. S1S0-I1, S1S0-I2, and S1S0-II. In the S_1 dynamic simulations, 54% trajectories decay to the S_0 state via S1S0-II; the remaining trajectories are de-excited to the S_0 state via S1S0-I1 (11%) and S1S0-I2 (35%). Our present theoretical investigation does not support the experimentally proposed S_1 excited-state hypothesis that the intramolecular rotation of the two dimethyl groups around the C-N bond is responsible for the rapid decay of the emission band at about 500 nm; instead, it should be heavily interrelated with the rotation of the two dimethylanilino groups. Finally, this work provides important mechanistic insights for similar diphenylmethane dyes.

Introduction

Due to their utility as molecular rotors, di- and tri-phenylmethane dyes such as malachite green, crystal violet, ethyl violet, and brilliant green have attracted a lot of experimental attention on their photophysical and photochemical properties.[1–25] In comparison, theoretical studies on these molecular rotors are rarely reported in the past decades.

Auramine-O, a representative diphenylmethane dye in Fig. 1, shows similar excited-state relaxation dynamics as has been reported for tri-phenylmethane dyes, especially its ultrafast photoinduced intramolecular conformational changes.[26–36] In the beginning, three important but different models were separately postulated by Oster and Nishijima,[37] Forster and Hoffmann,[38] and Bagchi, Fleming, and Oxtoby[39] to study the effect of viscosity on quantum yields and the barrierless torsional motion of phenyl groups that leads to a radiationless decay to the ground state. However, all these models can only describe a single-exponential excited-state relaxation behavior. Later, Martine and Glasbeek questioned the single-

exponential models on the basis of observing nonexponential excited-state behavior and proposed an adiabatic coupling model involving a locally emissive excited state and a nonemissive excited state.[40,41] Hirose et al. believed that not only solvent viscosity but also solvation dynamics affect the excited-state relaxation dynamics of Auramine-O.[42] Meech and coworkers proposed that in aqueous solution, solvation rather than solvent viscosity promotes a facile barrier-less formation charge-transfer state and decides the excited-state relaxation.[43,44] Singh et al. investigated Auramine-O using sub-picosecond time-resolved absorption spectroscopic techniques in aprotic and alcoholic solvents.[45,46] They found two different stimulated emission bands of ca. 715 and 830 nm and suggested there are two transition states involved in the excited-state relaxation. These findings oppose the widely accepted barrierless models. This is as well supported by Sen and Rafiq using time resolved femtosecond fluorescence measurements, in which an unexpectedly large fluorescence lifetime and multi-exponential transients in chloroform are observed.[47] They also found that Auramine-O has eight times larger fluorescence quantum yield in chloroform than in methanol and that the torsional motion of the dimethylanilino groups occurs in 1.5 ps in methanol and 14.2 ps in chloroform. More recently, Erez et al. employed steady-state and time-resolved optical techniques to study the short-time
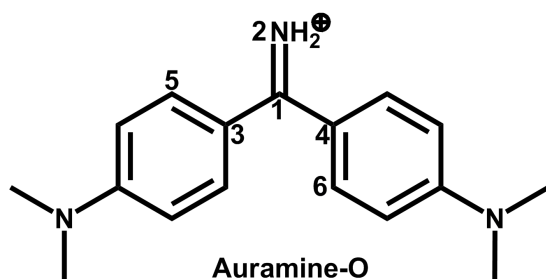
Fig. 1 Molecular structure of the diphenylmethane dye Auramine-O. Also shown are the atomic labeling and the dihedral angles ϕ_1 (N2C1C3C5), ϕ_2 (N2C1C4C6), and ϕ_3 (C3C1C4 N2).

excited-state decay dynamics of Auramine-O with a duration of about 150-300 fs in several solutions at room temperature.[48,49] They found that its excited-state behavior could be divided into three time steps. The shortest decay time constant is associated with a strong emission with a band maximum at about 500 nm, which is attributed to the twist motion of the dimethylamino group of the two anilines of Auramine-O. The second time constant is attributed to the rapid decay of the fluorescence band, which can be further red-shifted from about 510 nm to 550 nm in hydrogen-bonding solvents. The third time constant is related to a rather long decay of a dark state, about 10-20 ps in hydrogen-bonding liquids with medium viscosity. To summary, experimentally, there exist a few ambiguous even paradoxical viewpoints on the photophysical mechanism of Auramine-O. For example, whether is the torsional motion of the dimethylanilino groups barrierless in the S_1 state? what are the geometric and electronic structures for the transient states observed in experiments? what are the intrinsic S_1 excited-state deactivation paths? Obviously, answering these atomistic mechanistic details calls for high-level ab initio electronic structure calculations, even reliable nonadiabatic dynamics simulations.

However, to our best knowledge, there are only few theoretical works reported until now for excited-state properties of Auramine-O. Olsen proposed a four-electron, three-orbital model for low-energy electronic structures of several di- and tri-phenylmethane dyes including Auramine-O.[31] With DFT and TDDFT methods, Singh et al. obtained a ground state minimum and a transient state with emission maximum at 831 nm.[45] But, they did not obtain the other transient states proposed experimentally. Sen and Pafiq employed the same computational methods to scan the S_1 and S_0 potential energy surfaces of Auramine-O with respect to the rotation of the dimethylanilino rings.[47] In addition, they suggested a funnel for the S_1 excited-state radiationless decay to the ground state taking into account of the small S_1-S_0 energy gap.

In this work, we first emploit the complete active space self-consistent field (CASSCF) and its second-order perturba-

tion (CASPT2) methods to explore the S_1 excited-state minima, conical intersections, and potential energy profiles relevant to the excited-state decay. On the basis of the results, we propose our S_1 excited-state deactivation model. Finally, we use the semiempirical OM2/MRCI-based nonadiabatic dynamics simulations to verify our physical model. This work presents the first effort to systematically study the S_1 excited-state deactivation pathways of Auramine-O using combined high-level electronic structure calculations and nonadiabatic dynamics simulations, setting the stage for studying the photophysics of other similar diphenylmethane dyes in near future.

Simulation Details

Ab Initio Calculations

Ground-state conformer of Auramine-O is first optimized using the DFT method[50] with the B3LYP exchange-correlation functional.[51–54] Minima, conical intersections, and linearly interpolated internal coordinate (LIIC) paths are computed using the state-averaged complete active space self-consistent field (SA-CASSCF) method in which equal state weights are used for the S_1 and S_0 states. In the SA-CASSCF computations, the active space of 10 electrons in 8 orbitals is employed, which is referred to as SA-CASSCF(10,8) hereinafter. Since the CASSCF theory is unable to provide sufficient correlation energy, the multi-state complete active space 2nd-order perturbation approach (MS-CASPT2)[55,56] is exploited to re-evaluate the energies of all optimized structures and LIIC paths. In the MS-CASPT2 computations, the Cholesky decomposition technique with unbiased auxiliary basis sets is used for accurate two-electron integral approximations;[57] the ionization potential-electron affinity (IPEA) shift of 0.0 is used;[58] the imaginary shift technique (0.2 a.u.) is employed to avoid intruder-state issues.[59]

Vertical excitation energies at Franck-Condon points are also calculated using the MS-CASPT2, TD-B3LYP, and TD-CAM-B3LYP methods.[60,61] 6-31G and 6-31G* basis sets are employed for all geometry optimizations and single-point energy computations, respectively.[62–65] DFT and TD-DFT are carried out using GAUSSIAN09;[50,60,66] SA-CASSCF optimizations for conical intersections are performed using MOL-PRO2012;[67] all SA-CASSCF computations for minima and LIIC paths and MS-CASPT2 computations are conducted using MOLCAS8.0.[68,69]

Semiempirical Methods

All semiempirical calculations were performed using the OM2/MRCI method as implemented in the MNDO99 code.[70–73] During geometry optimizations and dynamics sim-

ulations, all required energies, gradients and nonadiabatic coupling elements were computed analytically. Minimum-energy conical intersections were optimized using the Lagrange-Newton approach. [74,75]

In the OM2/MRCI calculations, the restricted open-shell HF formalism was applied in the self-consistent field (SCF) treatment. The active space in the MRCI calculations included 12 electrons in 12 orbitals (see Supporting Information, Fig. S1). In terms of the SCF configuration it comprised five highest doubly occupied orbitals, two singly occupied orbitals, and five lowest unoccupied orbitals. For the MRCI treatment, three configuration state functions were chosen as references, namely the SCF configuration and the two closed-shell configurations derived therefrom (i.e., all singlet configurations that can be generated from HOMO and LUMO of the closed-shell ground state). The MRCI wavefunction was built by allowing all single and double excitations from these three references.

Nonadiabatic Dynamics

The S_1 nonadiabatic dynamics were studied by performing 1 ps OM2/MRCI trajectory surface-hopping simulations. The initial atomic coordinates and velocities for the S_1 photodynamics simulations were randomly selected from a 5 ps NVT (T=300K) ground-state trajectory. The excited states dynamics runs were then chosen according to the computed S_0-S_1 transition probabilities; configurations with very small S_0-S_1 transition dipole moments were not sampled. A total of 200 surface-hopping trajectories were run for the S_1 photodynamics, with all relevant energies, gradients, and nonadiabatic coupling vectors being computed on-the-fly as needed. For points with an energy gap of less than 10 kcal/mol, the fewest-switches criterion was applied to decide whether to hop. The time step was chosen to be 0.1 fs for the nuclear motion and 0.0005 fs for the electronic propagation. The unitary propagator evaluated at mid-point was used to propagate the electronic motion. The translational and rotational motions were removed in each step. The empirical decoherence correction (0.1 au) proposed by Granucci et al. was employed. [76] The final evaluations were done for 186 trajectories that finished successfully in the S_1 photodynamics and that satisfied our energy continuity criterion (no change greater than 30 kcal/mol between any two consecutive MD steps). Further technical details were given in previous publications. [25,77–98]

Results and Discussion

S_0 Structure and Vertical Excitation Energies

By using the OM2/MRCI and SA-CASSCF methods, we have optimized the ground-state conformers of Auramine-O. All these computations give similar equilibrium structure in Fig.

Table 1 Vertical Excitation Energies (in eV) to the S_1 State; Experimental Values Are Measured in Methanol. [49]

	OM2/MRCI[a]	MS-CASPT2[b]	Exp.
S_1	2.6	2.6	3.0

[a]OM2/MRCI optimized S_0 minimum structure;
[b]SA-CASSCF optimized S_0 minimum structure.

3. The stable S_0 conformer is almost in C_2 symmetry. Its C1-C3 and C1-C4 bond lengths are 1.439 and 1.440 Å at the SA-CASSCF level, as well as its two dihedral angles ϕ_1(N2C1C3C5) and ϕ_2(N2C1C4C6), which are computed to be 29.8° and 29.2° at the same computational level.

Table 1 collects the computed vertical excitation energies to S_1 at the S_0 minimum S0. Compared with the experimental value measured in methanol solution, [49] TD-CAM-B3LYP and MS-CASPT2 computations overestimate and underestimate the $S_0 \rightarrow S_1$ vertical excitation energy, respectively; but, TD-B3LYP computations fortuitously give very good agreement. Our current OM2/MRCI computations give reasonably accurate number: the vertical excitation energy to the S_1 state is 0.4 eV lower than the experimental value. [49]

Analysis of electronic configuration states in the CASPT2 computations illustrates that the S_1 vertical electronic excitation mainly originates from HOMO→LUMO in Fig. 2 (weight: 0.67) and HOMO-1→LUMO (0.16). The S_1 electronic state at the Franck-Condon point is of clear charge-transfer character from the phenyl to methaniminium group. Charge-transfer electronic transition is usually associated with the remarkable change of permanent electronic dipole moments, either magnitudes or directions. In our OM2/MRCI computations, electronic dipole moments at the S_0 minimum S0 are computed to be 2.2 Debye for the S_0 state and 1.2 Debye for the S_1 state; thus, the S_1 state is of charge-transfer character. It is in line with the point of view proposed by Singh et al. [45] that the emissive state is expected to be less polar than the ground state due to the neutralization of positive charge of the nitrogen atom as a result of intramolecular charge transfer from the dimethylanilino to methaniminium or imidocarbonyl group.

S_1 Minima

With the OM2/MRCI and SA-CASSCF methods, three kinds of minima are optimized in the S_1 state, which are referred to as S1-LE, S1-I1, S1-I2, and S1-II in Fig. 3. Overall, S1-LE is structurally similar to the S_0 minimum S0 except a little different bond lengths and dihedral angles. In comparison, S1-II changes a lot in structure. At the OM2/MRCI and SA-CASSCF levels, the corresponding ϕ_1 and ϕ_2 dihedral angles are $\phi_1 = 127.8°$ and 128.1°, and $\phi_2 = 33.9°$ and 34.9°; the
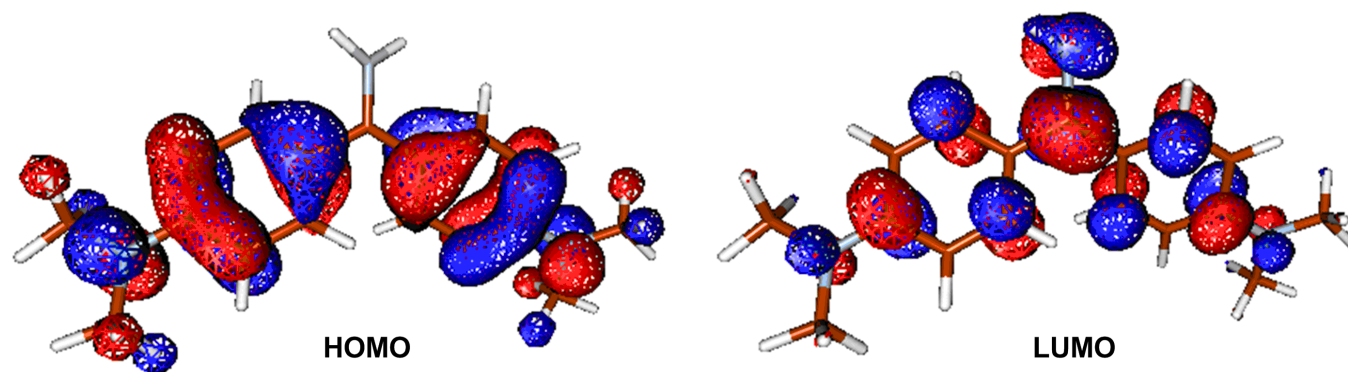
HOMO   **LUMO**

Fig. 2 Canonical molecular orbitals related to the $S_0 \rightarrow S_1$ (HOMO→LUMO) electronic transition at the Franck-Condon point at the OM2/MRCI level.

Table 2 OM2/MRCI [MS-CASPT2] Computed Relative Energies (in kcal/mol) of All OM2/MRCI [CASSCF] Optimized Structures

structure	S0	S1-LE	S1-I1	S1-I2
OM2/MRCI	0.0	62.5	62.2	62.2
MS-CASPT2	0.0	60.0	68.1	68.1
structure	S1-II	S1S0-I1	S1S0-I2	S1S0-II
OM2/MRCI	60.4	66.5	67.2	62.5
MS-CASPT2	64.5	74.0	74.3	69.2

C1-C3 and C1-C4 bond lengths are nearly same to each other, 1.486 and 1.484 , and 1.484 and 1.485 , respectively. Its dihedral angle ϕ_3 is also rotated to about 137.0° and 138.9° as the central carbon atom changes its hybridization pattern from sp^2 to sp^3. In addition, we have also optimized another pair of S_1 minima i.e. S1-I1 and S1-I2 in Fig. 3. In these two structures, one aminophenyl group is almost perpendicular to the other aminophenyl and amino groups, for example, $\phi_2 = 103.6°$ (101.1°) for S1-I1 and $\phi_1 = 74.6°$ (77.2°) in S1-I2 at the OM2/MRCI (SA-CASSCF) level. Energetically, these four S_1 minima are close to each other: in the order of S1-LE, S1-I1, S1-I2, and S1-II, they are 62.5 (60.0), 62.2 (68.1), 62.2 (68.1), and 60.4 (64.5) kcal/mol at the OM2/MRCI (MS-CASPT2) level. However, their importances in the photodynamics of Auramine-O are very different due to the ease of access to these structures (see the following).

In experiments of steady-state absorption and emission spectra in different solutions, Palit and coworkers found an important spectroscopic feature that there is a weak but long tail for the main fluorescence band, which is beyond 800 nm.[45] The main intense emission band centered at 495 nm was experimentally assigned to a locally excited electronic state; the weak one to a relaxed weakly emissive excited state. In addition, on the basis of time-resolved absorption-stimulated emis-

sion spectra, Palit et al. also suggested that the relaxation process proceeds via the formation of at least two transient states, which are geometrical conformers and consecutively formed following the decay of the local excited state. The steady-state fluorescence spectra show three emission bands centered at 510 nm, 710 nm and 870 nm, respectively. All experimental information implies that there exist at least three S_1 minima. However, only a transient state was obtained up to date computationally at the TD-DFT level.[45] The electronic and geometric structures of the other emissive states are not known. Here we have for the first time assigned these three emission bands. The emission band at S1-LE is computed to be 523 nm with oscillator strength of 0.84 at the MS-CASPT2 level. This should correspond to the intense emission band of the locally excited electronic state observed in experiments (510 nm). Similarly, both emission bands of S1-I1 and S1-I2 are calculated to be 721 nm with oscillator strengths of 0.10, which match very well with the weak emission bands of 710 nm. The emission band of S1-II is predicted to be 884 nm with oscillator strength of 0.06 at the MS-CASPT2 level, which should correspond to the weakest emission band around 870 nm in experiments.[45]

S_1/S_0 Conical Intersections

In addition, we have obtained three S_1/S_0 conical intersections, which are labeled as S1S0-I1, S1S0-I2, and S1S0-II in Fig. 3. Structurally, they are respectively close to their corresponding S_1 minima, for example S1S0-I1 close to S1-I1. Energetically, S1S0-II is the lowest among these three conical intersections: it is about 4.0 (4.8) and 4.7 (5.1) kcal/mol lower than S1S0-I1 and S1S0-I2 at the OM2/MRCI (MS-CASPT2) level. All these three S_1/S_0 conical intersections are energetically accessible because they are just ca. 5 kcal/mol higher than their related S_1 minima in energy. On the other side, the computed LIIC paths also show that S1S0-I1, S1S0-I2, and
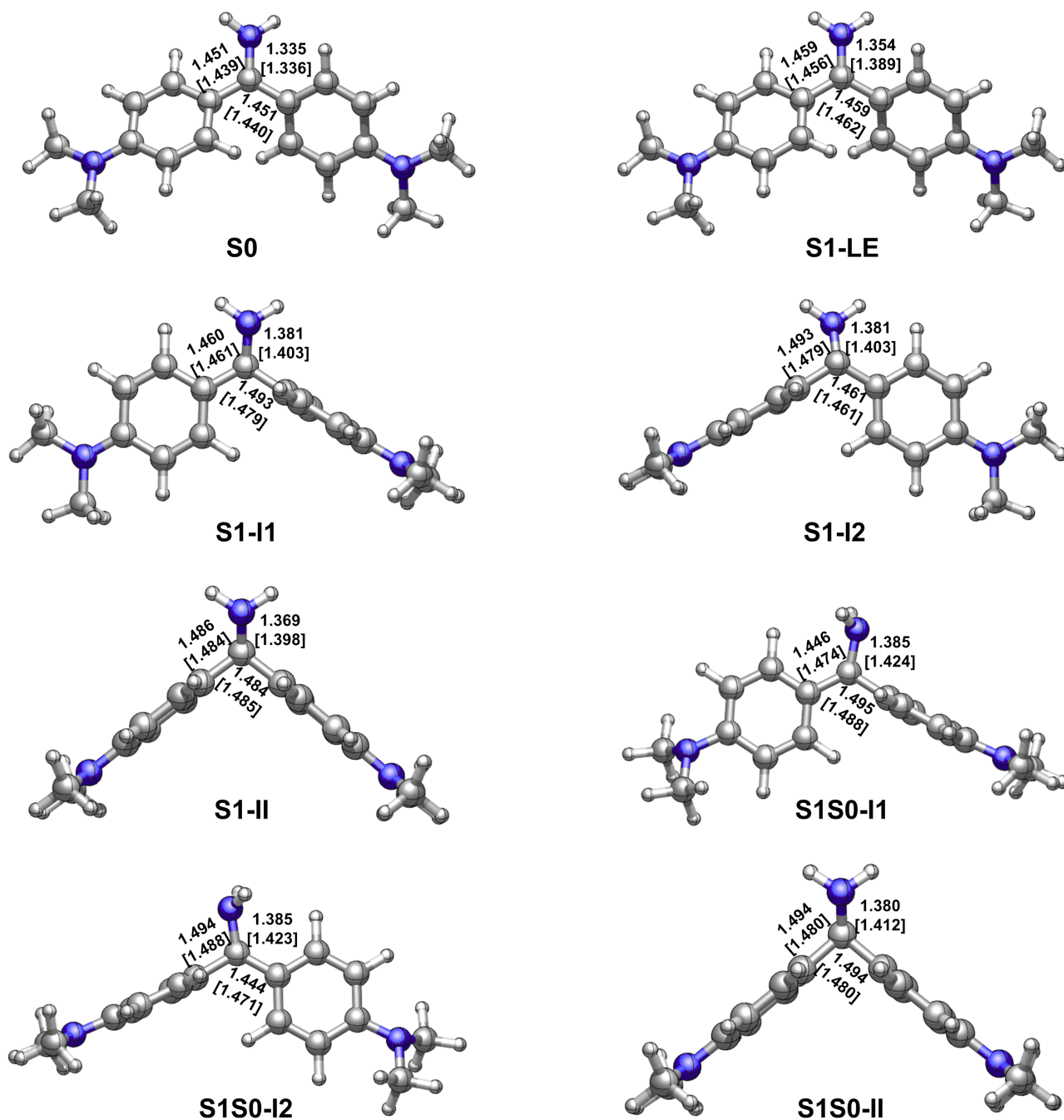
Fig. 3 OM2/MRCI [SA-CASSCF] optimized S_0 and S_1 minima, and S_1/S_0 conical intersections. See Table 2 for their relative energies and Fig. 1 for the dihedral angles ϕ_1 (N2C1C3C5), ϕ_2 (N2C1C4C6), and ϕ_3 (C3C1C4 N2).
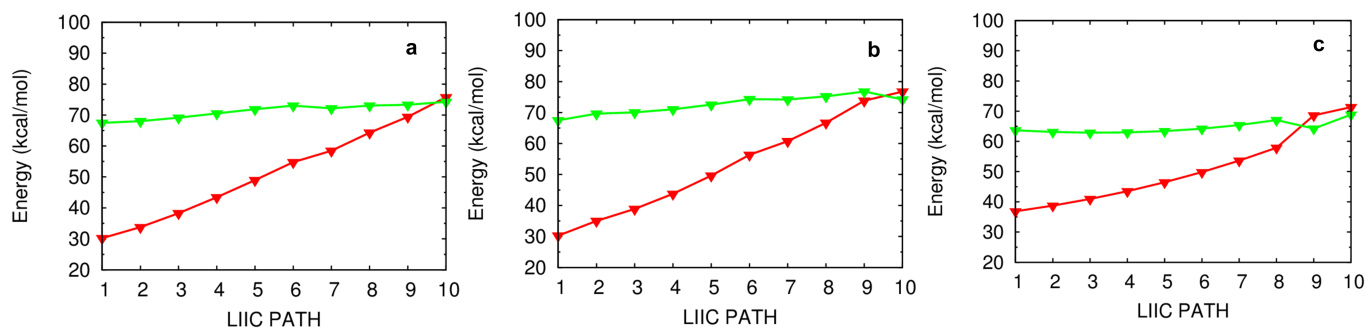
Fig. 4 Linearly interpolated internal coordinate (LIIC) paths connecting (a) S1-II and S1S0-II; (b) S1-I1 and S1S0-I1; (c) S1-I2 and S1S0-I2.

S1S0-II can be approached readily from the corresponding S_1 minima (see panel a, b, and c in Fig. 4).

Nonadiabatic Dynamics

On the basis of the results of static electronic structure computations, one can see that the chosen OM2/MRCI method gives reasonably accurate S_1 excited-state electronic and geometric structures in comparison to those computed by the SA-CASSCF method. More important for photodynamics simulations is that the OM2/MRCI method can accurately describe the conical intersections among the lowest two singlet states of Auramine-O, i.e. S_0 and S_1. In the following, the OM2/MRCI method is exploited to simulate the photodynamics of Auramine-O starting from the initial S_1 excited state.

Among 186 trajectories in the S_1 nonadiabatic dynamics simulations, 46 trajectories decay to the S_0 state at the end of 1 ps; while, 140 trajectories survive in the S_1 state. Fig. 5 shows the time-dependent S_1 and S_0 state populations. In the first 260 fs, both state populations do not change at all. This period of time should correspond to the initial relaxation time from the S_1 Franck-Condon point via the S_1 minima to the S_1/S_0 conical intersections. This process takes a relatively long time because such process involves marked conformational change, e.g. ϕ_1 changes from 28.6° of S0 to 135.6° of S1S0-II. After this relaxation, the S_1 system starts to decay gradually to the S_0 state until the end of simulations.

If the S_1 excited-state decay is treated as a first-order process, we can estimate the S_1 excited-state lifetime τ to be about 3.6 ps according to the single-exponential fitting equation of $p = exp(-(t - t_0)/\tau) + p_0$, in which the initial delay time t_0 and the residual S_1 state population p_0 are assigned to 258.8 fs and 0.8, respectively.

The distribution of the selected dihedral angles ϕ_1 and ϕ_2 at all $S_1 \rightarrow S_0$ hopping points in the S_1 photodynamics is shown in Fig. 6. The dihedral angles ϕ_1 (N2C1C3C5) and ϕ_2 (N2C1C4C6) are mainly distributed around 40-70° and 110-140°, respectively. Such distribution is consistent with the S_1
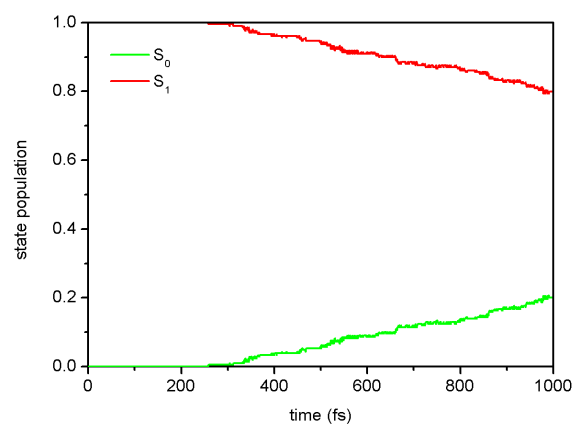
Fig. 5 Time-dependent S_1 and S_0 state populations in the two-state (S_1 and S_0) photodynamics simulations.

	N2C1C3C5	N2C1C4C6
S1S0-I1	18.5°	97.5°
S1S0-I2	97.3°	19.0°
S1S0-II	135.6°	48.7°
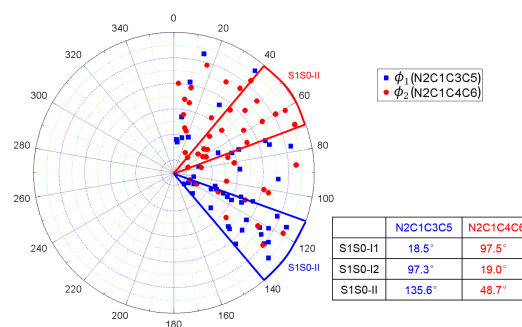
Fig. 6 Distribution of the dihedral angles ϕ_1 (N2C1C3C5) and ϕ_2 (N2C1C4C6) at the $S_1 \rightarrow S_0$ hopping points.

Table 3 Averaged $S_1 \rightarrow S_0$ Hopping Times (unit: fs) via S1S0-I1, S1S0-I2, and S1S0-II.

	S1S0-I1	S1S0-I2	S1S0-II
t	441	597	716

excited-state topological structures computed in the preceding static electronic structure calculations (see above). S1S0-II is energetically lowest among the three S_1/S_0 conical intersections: it is about 5.0 kcal/mol lower than the other two at the OM2/MRCI and MS-CASPT2 levels (see Table 2). In addition, for our case, along the ϕ_1 and ϕ_2 dihedral angles, the S_1-S_0 energy gap is very small; the S_1 potential energy surface is very flat and forms an extended conical intersection seam with the S_0 state. Therefore, the distribution of these two angles at the hopping points is much spread.

It is found from Fig. 7 that 54% hopping-trajectories decay to the S_0 state via S1S0-II; and, 11% and 35% hopping-trajectories do via S1S0-I1 and S1S0-I2. How to understand this distribution? First, energetically, S1S0-II is the lowest one among the three S_1/S_0 conical intersections; the former is computed to be about 5.0 kcal/mol lower than the latter two at both OM2/MRCI and MS-CASPT2 levels. Thus, we can understand very well that the preferred $S_1 \rightarrow S_0$ hopping region is close to S1S0-II. Second, why is S1S0-I2 superior to S1S0-I1 for the S_1 excited-state deactivation although both conical intersections have nearly same potential energies? It is clear that upon irradiation to the S_1 state, the lowest S_1 minimum S1-LE is first populated because S1-LE is structurally more close to the Franck-Condon point i.e. the S_0 minimum S0 (see Fig. 3). At this point, except proceeding to S1-II, there still exist two other excited-state relaxation paths, first to S1-I1 and second to S1-I2. However, as shown in Fig. 8, the conformational change from S1-LE to S1-I2 is significantly smaller than that from S1-LE to S1-I1. Therefore, more trajectories will decay to the S_0 state around S1-I2 via S1S0-I2. In addition, we have computed the averaged $S_1 \rightarrow S_0$ hopping times via S1S0-I1, S1S0-I2, and S1S0-II, which are 441, 597, and 716 fs, respectively (Table 3).

Typical Trajectories

It is noteworthy that starting from the locally excited S_1 minimum S1-LE, there exist three competitive S_1 relaxation processes (two sequential and one concerted paths; see panal a of Fig. 9).

The first two relaxation processes are related to the rotation of two dimethylanilino groups (ϕ_1 and ϕ_2), as shown in panel b and c of Fig. 9. In these two paths, the system near the locally excited S_1 minimum first proceeds into a transient excited-state intermediate S1-I1 or S1-I2 via a simple rotation
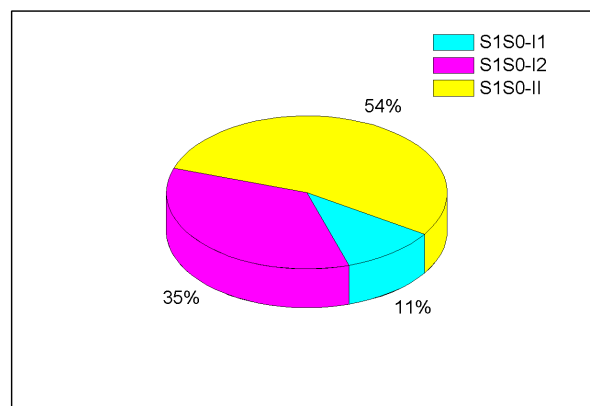
Fig. 7 Percentage distribution of the $S_1 \rightarrow S_0$ hoppings via S1S0-I1, S1S0-I2, and S1S0-II conical intersections in the photodynamics of Auramine-O.

of a dimethylanilino group. These two intermediates S1-I1 and S1-I2 are spectroscopically observed in experiments (see above discussion). After arriving at S1-I1 or S1-I2, the system not only can decay to the S_0 state via the nearby S_1/S_0 conical intersections S1S0-I1 or S1S0-I2 but also can further evolve into the S_1 minimum S1-II by rotating the remaining dimethylanilino group (transient state II in experiments). Finally, the system is de-excited via another S_1/S_0 conical intersection S1S0-II returning back the S_0 state. Certainly, in addition to the sequential paths to S1-II, from the locally S_1 excited-state minimum S1-LE the system can also, bypassing S1-I1 and S1-I2, concertedly proceed into the final transient S_1 excited-state minimum S1-II.

Fig. 10 shows the time-dependent evolution of the two dihedral angles ϕ_1 and ϕ_2 and the S_1-S_0 nonadiabatic coupling in three trajectories that support the sketch in Fig. 9. Panel a and b represent the sequential S_1 relaxation paths. As shown in panel a, in the first 380 fs, the ϕ_2 dihedral angle gradually decreases to about $70°$ from the initial $160°$; while, the corresponding ϕ_1 dihedral angle just oscillates around its equilibrium value. At that time, the system still encounters a conical intersection region with large nonadiabatic coupling. However, the system does not hop to the S_0 state; instead, it continues to evolve into the S1-II region through rotating the ϕ_1 dihedral angle. Near this region, the S_1 system jumps to the ground state at 481 fs. The dynamical bahavior of the trajectory in panel b of Fig. 10 is similar to that in panel a, except rotating the two dihedral angles ϕ_1 and ϕ_2 in a different order. In contrast, in panel c, the rotations of these two dihedral angles proceed in a synchronous means; hence, the system in this trajectory directly runs into the S1-II region, near which the S_0 state is populated at 553 fs as a result of the $S_1 \rightarrow S_0$
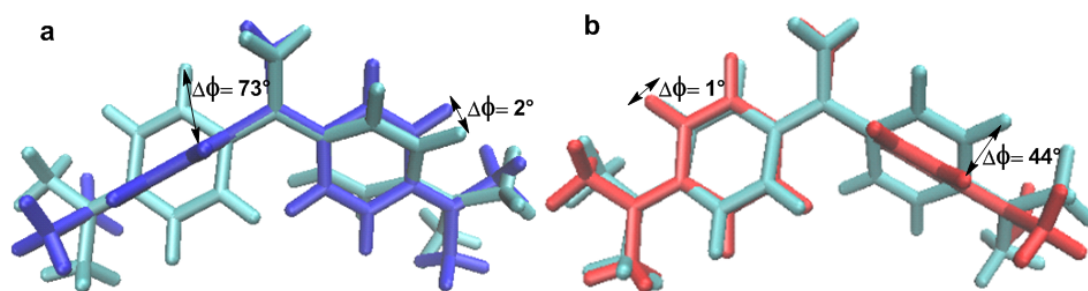
Fig. 8 Spatial overlap of the three different S_1 geometric structures produced by the VMD1.9.1 package [99]: (a) S1-LE and S1-I1 and (b) S1-LE and S1-I2.

internal conversion. Finally, it must be stressed that in our simulations, most of trajectories decay to the ground state using the concerted way and only a few ones decay to S_0 via the sequential means.

Correlation with Experiments

On the basis of the results of present static electronic structure calculations and dynamics simulations, we have gained several new mechanistic insights for the photophysics of Auramine-O.

First, we have for the first time computationally characterized the three S_1 excited-state transient states observed in the subpicosecond time-resolved spectroscopic experiments of Singh et al. [45] (see above; Fig. 9).

Second, the emission band of ca. 500 nm observed in the steay-state and time-resolved experiments of Erez et al., [49] in terms of our computational results, should be assigned to the locally excited transient state.

Third, in addition to the experimentally proposed sequential S_1 relaxation process leading to the transient intermediate S1-II (referred to as TS II in experiments), we have observed a concerted S_1 relaxation path to S1-II. This explains why the S_1 relaxation process exhibits a multi-exponential excited-state dynamics behavior. [45]

Forth, the S_1 excited-state decay is experimentally proposed to occur primarily near S1-II. [45] However, the corresponding S_1/S_0 conical intersection is not characterized computationally unitl now. Here, we not only optimized this conical intersection but also found the other two S_1/S_0 conical intersections in the vicinity of S1-I1 and S1-I2. The importance of these three conical intersections in the S_1 excited-state decay of Auramine-O has been proved in our nonadiabatic dynamics simulations. It is found that S1S0-II plays a major role for the S_1 excited-state decay; but, the significance of the other two conical intersections S1S0-I1 and S1S0-I2 cannot be excluded as well, which accounts for 46% of all trajectories that decay to the S_0 state.

Fifth, in a recent experimental study, Erez et al. proposed an S_1 excited-state deactivation mechanism: the intramolecular rotation of the dimethyl groups around the C-N bond is responsible for the rapid decay (150-300 fs) of the emission band at about 500 nm. [49] This mechanism is not supported by our present electronic structure calculations and nonadiabatic dynamics simulations; instead, the S_1 excited-state decay should be heavily interrelated with the rotation of the dimethylanilino groups, which is consistent with experiments of Rafiq et al. [47] and Singh et al. [45]

Conclusions

With the use of high-level MS-CASPT2//CASSCF electronic structure calculations and semi-empirical OM2/MRCI nonadiabatic dynamics simulations, we have for the first time theoretically explored the S_1 excited-state deactivation mechanism of Auramine-O. First, the S_1 excited-state minima, the S_1/S_0 conical intersections, and the relevant S_1 excited-state potential energy profiles are computed at the MS-CASPT2//CASSCF and OM2/MRCI levels. On the basis of these static electronic structure calculations, we have assigned all three transient states proposed in experiments [45] and suggested an S_1 excited-state decay mechanism involving three S_1 transient intermediate states and three S_1/S_0 conical intersections. Our proposed S_1 decay mechanism is immediately verified by our following OM2/MRCI-based surface-hopping dynamics simulations. In addition, we have found that the S_1 relaxation process to the final transient state can proceed either sequentially or concertedly. This work represents the first theoretical effort to explore the S_1 excited-state deactivation processes of diphenylmethane dyes.

Acknowledgments
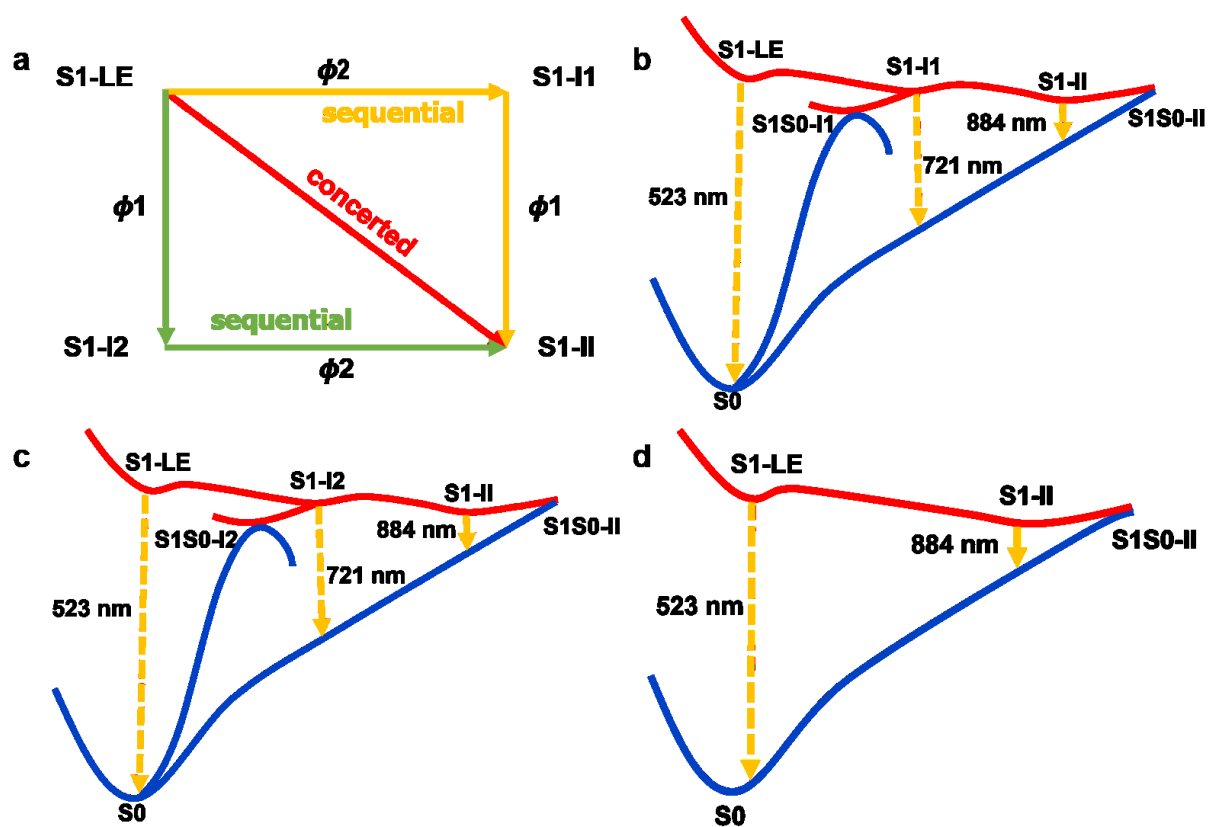
Fig. 9 Concerted and sequential deactivation channels proposed based on the present electronic structure calculations and nonadiabatic dynamics simulations. See text for discussion.
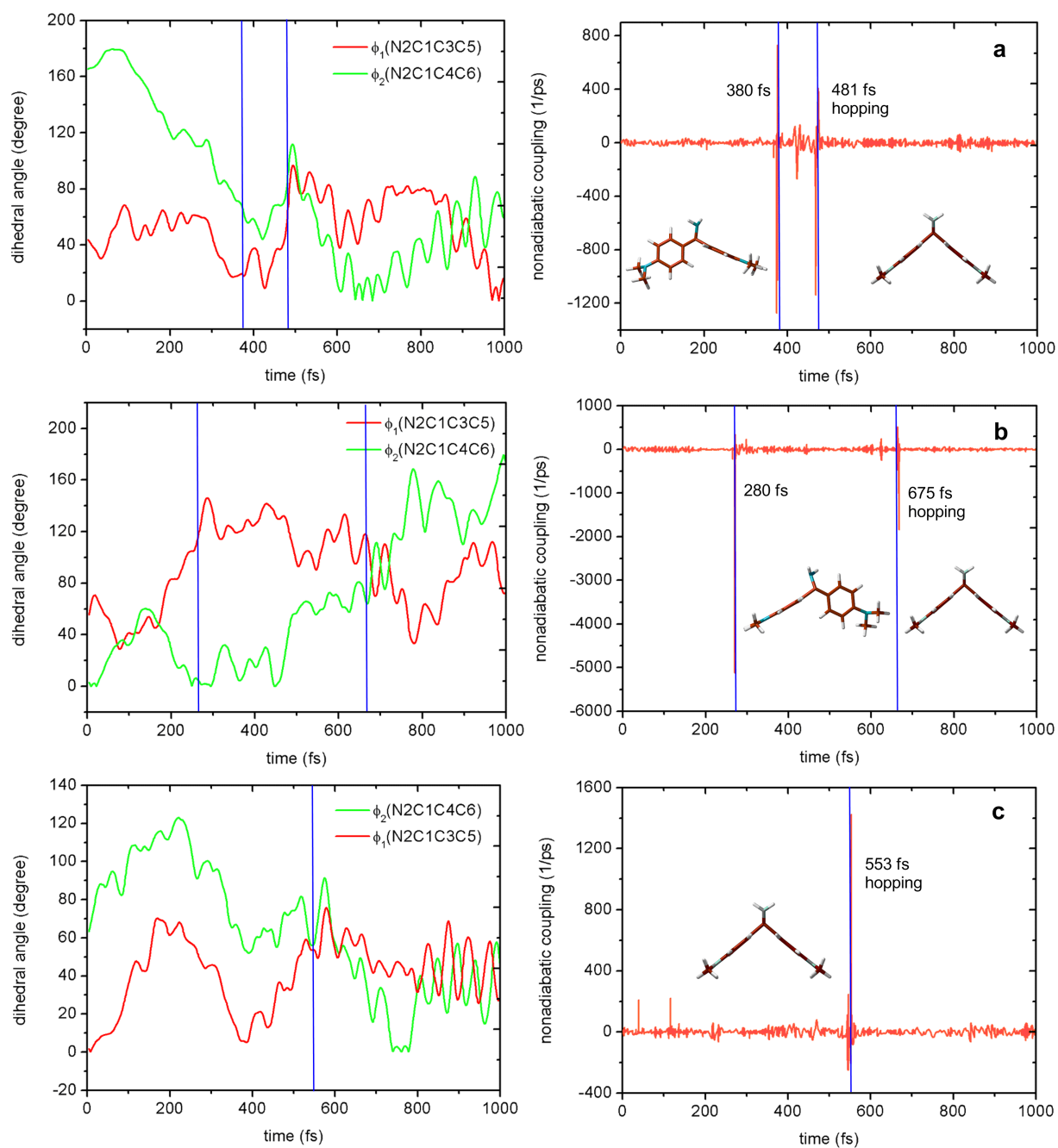
Fig. 10 Three representative trajectories. In panel a and b, the S$_1$ system first evolves to the transient intermediates S1-I1 or S1-I2 and then to the final transient state S1-II; in panel c, the system concertedly, bypassing S1-I1 amd S1-I2, proceeds into the final transient S$_1$ excited-state minimum S1-II.

perts" and "Fundamental Research Funds for Central Universities".

Supporting Information

Active orbitals in the OM2/MRCI and CASSCF computations, and Cartesian coordinates of all optimized structures and LIIC paths. This material is available free of charge via the Internet at http://pubs.acs.org.

References

1 W. Yu, F. Pellegrino, M. Grant and R. R. Alfano, *J. Chem. Phys.*, 1977, **67**, 1766–1773.

2 J. M. Grzybowski, S. E. Sugamori, D. F. Williams and R. W. Yip, *Chem. Phys. Lett.*, 1979, **65**, 456–460.

3 D. A. Cremers and M. W. Windsor, *Chem. Phys. Lett.*, 1980, **71**, 27–32.

4 R. Menzel, C. W. Hoganson and M. W. Windsor, *Chem. Phys. Lett.*, 1985, **120**, 29–34.

5 M. Vogel and W. Rettig, *Ber. Bunsen-Ges. Phys. Chem*, 1985, **89**, 962–968.

6 A. Mokhtari, L. Fini and J. Chesnoy, *J. Chem. Phys.*, 1987, **87**, 3429–3435.

7 F. W. Wise, M. J. Rosker and C. L. Tang, *J. Chem. Phys.*, 1987, **86**, 2827–2832.

8 M. Canva, G. Le Saux, P. Georges, A. Brun, F. Chaput and J. P. Boilot, *Chem. Phys. Lett.*, 1991, **176**, 495–498.

9 M. Ishikawa and Y. Maruyama, *Chem. Phys. Lett.*, 1994, **219**, 416–420.

10 K. M. Abedin, J. Y. Ye, H. Inouye, T. Hattori, H. Sumi and H. Nakatsuka, *J. Chem. Phys.*, 1995, **103**, 6414–6425.

11 Y. Maruyama, M. Ishikawa and H. Satozono, *J. Am. Chem. Soc.*, 1996, **118**, 6257–6263.

12 J. Y. Ye, T. Hattori, H. Inouye, H. Ueta, H. Nakatsuka, Y. Maruyama and M. Ishikawa, *Phys. Rev. B: Condens. Matter*, 1996, **53**, 8349–8353.

13 J. Y. Ye, T. Hattori, H. Nakatsuka, Y. Maruyama and M. Ishikawa, *Phys. Rev. B*, 1997, **56**, 5286–5296.

14 B. Strehmel, H. Seifert and W. Rettig, *J. Phys. Chem. B*, 1997, **101**, 2232–2243.

15 A. C. Bhasikuttan, L. V. Shastri, A. V. Sapre and J. P. Mittal, *J. Photochem. Photobiol., A*, 1998, **112**, 179–185.

16 J. Y. Ye, M. Ishikawa, O. Yogi, T. Okada and Y. Maruyama, *Chem. Phys. Lett.*, 1998, **288**, 885–890.

17 M. Ishikawa, J. Y. Ye, Y. Maruyama and H. Nakatsuka, *J. Phys. Chem. A*, 1999, **103**, 4319–4331.

18 M. Jurczok, P. Plaza, M. M. Martin and W. Rettig, *J. Phys. Chem. A*, 1999, **103**, 3372–3377.

19 Y. Maruyama, O. Magnin, H. Satozono and M. Ishikawa, *J. Phys. Chem. A*, 1999, **103**, 5629–5635.

20 Y. Kanematsu, H. Ozawa, I. Tanaka and S. Kinoshita, *J. Lumin.*, 2000, **87-9**, 917–919.

21 M. Glasbeek and H. Zhang, *Chem. Rev.*, 2004, **104**, 1929–1954.

22 M. Kondo, I. A. Heisler, J. Conyard, J. P. H. Rivett and S. R. Meech, *J. Phys. Chem. B*, 2009, **113**, 1632–1639.

23 M. Kondo, I. A. Heisler and S. R. Meech, *Faraday Discuss.*, 2010, **145**, 185–203.

24 S. Rafiq, B. K. Rajbongshi, N. N. Nair, P. Sen and G. Ramanathan, *J. Phys. Chem. A*, 2011, **115**, 13733–13742.

25 B. B. Xie, S. H. Xia, L. H. Liu and G. L. Cui, *J. Phys. Chem. A*, 2015, **119**, 5607–5617.

26 P. Changenet, H. Zhang, M. J. Van Der Meer, M. Glasbeek, P. Plaza and M. M. Martin, *J. Phys. Chem. A*, 1998, **102**, 6716–6721.

27 P. Changenet, H. Zhang, M. J. van der Meer, M. Glasbeek, P. Plaza and M. M. Martin, *J. FLUORESC.*, 2000, **10**, 155–160.

28 N. Forsberg and P. A. Malmqvist, *Chem. Phys. Lett.*, 1997, **274**, 196–204.

29 M. Hasegawa, T. Sugimura, Y. Suzaki, Y. Shindo and A. Kitahara, *J. Phys. Chem.*, 1994, **98**, 2120–2124.

30 N. T. Hunt, A. A. Jaye and S. R. Meech, *Chem. Phys. Lett.*, 2005, **416**, 89–93.

31 S. Olsen, *J. Phys. Chem. A*, 2012, **116**, 1486–1492.

32 P. Prosposito, H. Zhang and M. Glasbeek, *J. Sol-Gel. Sci. Techn.*, 2011, **60**, 347–351.

33 R. F. Steiner, S. Albaugh, E. Nenortas and L. Norris, *Biopolymers*, 1992, **32**, 73–83.

34 S. R. Valandro, A. L. Poli, M. G. Neumann and C. C. Schmitt, *J. Lumin.*, 2015, **161**, 209–213.

35 Y. Wang and H. Morawetz, *Macromolecules*, 1986, **19**, 1925–1930.

36 J. G. Weers and A. H. Maki, *Biochemistry*, 1986, **25**, 2897–2904.

37 G. Oster and Y. Nishijima, *J. Am. Chem. Soc.*, 1956, **78**, 1581–1584.

38 T. Förster and G. Hoffmann, *Z. Phys. Chem., Neue Folge*, 1971, **75**, 63–76.

39 B. Bagchi, G. R. Fleming and D. W. Oxtoby, *J. Chem. Phys.*, 1983, **78**, 7375–7385.

40 M. Glasbeek, H. Zhang and M. J. Van der Meer, *J. Mol. Liq.*, 2000, **86**, 123–126.

41 M. J. Van Der Meer, H. Zhang and M. Glasbeek, *J. Chem. Phys.*, 2000, **112**, 2878–2887.

42 Y. Hirose, H. Yui and T. Sawada, *J. Phys. Chem. B*, 2004, **108**, 9070–9076.

43 I. A. Heisler, M. Kondo and S. R. Meech, *J. Phys. Chem. B*, 2009, **113**, 1623–1631.

44 M. Kondo, I. A. Heisler and S. R. Meech, *J. Mol. Liq.*, 2012, **176**, 17–21.

45 C. Singh, B. Modak, J. A. Mondal and D. K. Palit, *J. Phys. Chem. A*, 2011, **115**, 8183–8196.

46 P. K. Singh, A. K. Mora, S. Murudkar and S. Nath, *RSC Adv.*, 2014, **4**, 34992–35002.

47 S. Rafiq and P. Sen, *J. Chem. Phys.*, 2013, **139**, 124302–124309.

48 Y. Erez, N. Amdursky, R. Gepshtein and D. Huppert, *J. Phys. Chem. A*, 2012, **116**, 12056–12064.

49 Y. Erez, R. Simkovitch, K. Akulov, R. Gepshtein, T. Schwartz and D. Huppert, *J. Phys. Chem. C*, 2014, **118**, 27063–27073.

50 R. G. Parr and W. T. Yang, *Density-Functional Theory of Atoms and Molecules*, Oxford University Press, USA, 1994.

51 S. H. Vosko, L. Wilk and M. Nusair, *Can. J. Phys.*, 1980, **58**, 1200–1211.

52 C. Lee, W. T. Yang and R. G. Parr, *Phys. Rev. B*, 1988, **37**, 785–789.

53 A. D. Becke, *Phys. Rev. A*, 1988, **38**, 3098–3100.

54 A. D. Becke, *J. Chem. Phys.*, 1993, **98**, 1372–1377.

55 K. Andersson, P. A. Malmqvist, B. O. Roos, A. J. Sadlej and K. Wolinski, *J. Phys. Chem.*, 1990, **94**, 5483–5488.

56 K. Andersson, P. Å. Malmqvist and B. O. Roos, *J. Chem. Phys.*, 1992, **96**, 1218–1226.

57 F. Aquilante, R. Lindh and T. Bondo Pedersen, *J. Chem. Phys.*, 2007, **127**, 114107–114113.

58 G. Ghigo, B. O. Roos and P. Malmqvist, *Chem. Phys. Lett.*, 2004, **396**, 142–149.

59 N. Försberg and P. Å. Malmqvist, *Chem. Phys. Lett.*, 1997, **274**, 196–204.

60 M. A. L. Marques, C. A. Ullrich, F. Nogueira, A. Rubio, K. Burke and E. K. U. Gross, *Time-dependent Density Functional*, Springer, 2006.

61 T. Yanai, D. P. Tew and N. C. Handy, *Chem. Phys. Lett.*, 2004, **393**, 51–57.

62 R. Ditchfield, W. J. Hehre and J. A. Pople, *J. Chem. Phys.*, 1971, **54**, 724–728.

63 M. M. Francl, W. J. Pietro, W. J. Hehre, J. S. Binkley, M. S. Gordon, D. J. DeFrees and J. A. Pople, *J. Chem. Phys.*, 1982, **77**, 3654–3665.

64 G. L. Cui, P. J. Guan and W.-H. Fang, *J. Phys. Chem. A*, 2014, **118**, 4732–4739.

65 P. J. Guan, G. L. Cui and Q. Fang, *ChemPhysChem*, 2015, **16**, 805–811.

66 M. J. Frisch, G. W. Trucks, H. B. Schlegel, G. E. Scuseria, M. A. Robb, J. R. Cheesem, G. Scalmani, V. Barone, B. Mennucci, G. A. Petersson, H. Nakatsuji, M. Caricato, X. Li, H. P. Hratchian, A. F. Izmaylov, J. Bloino, G. Zheng, J. L. Sonnenberg, M. Hada, M. Ehara, K. Toyota, R. Fukuda, J. Hasegawa, M. Ishida, T. Nakajima, Y. Honda, O. Kitao, H. Nakai, T. Vreven, J. A. M. Jr., J. E. Peralta, F. Ogliaro, M. Bearpark, J. J. Heyd, E. Brothers, K. N. Kudin, V. N. Staroverov, R. Kobayashi, J. Normand, K. Raghavachari, A. Rendell, J. C. Burant, S. S. Iyengar, J. Tomasi, M. Cossi, N. Rega, J. M. Millam, M. Klene, J. E. Knox, J. B. Cross, V. Bakken, C. Adamo, J. Jaramillo, R. Gomperts, R. E. Stratmann, O. Yazyev, A. J. Austin, R. Cammi, C. Pomelli, J. W. Ochterski, R. L. Martin, K. Morokuma, V. G. Zakrzewski, G. A. Voth, P. Salvador, J. J. Dannenberg, S. Dapprich, A. D. Daniels, O. Farkas, J. B. Foresman, J. V. Ortiz, J. Cioslowski and D. J. Fox, *Gaussian 09, Revision A.02*, Gaussian, Inc., Wallingford CT, 2009.

67 H.-J. Werner, P. J. Knowles, G. Knizia, F. R. Manby, M. Schütz, P. Celani, T. Korona, R. Lindh, A. Mitrushenkov, G. Rauhut, K. R. Shamasundar, T. B. Adler, R. D. Amos, A. Bernhardsson, A. Berning, D. L. Cooper, M. J. O. Deegan, A. J. Dobbyn, F. Eckert, E. Goll, C. Hampel, A. Hesselmann, G. Hetzer, T. Hrenar, G. Jansen, C. Köppl, Y. Liu, A. W. Lloyd, R. A. Mata, A. J. May, S. J. McNicholas, W. Meyer, M. E. Mura, A. Nicklass, D. P. O'Neill, P. Palmieri, D. Peng, K. Pflüger, R. Pitzer, M. Reiher, T. Shiozaki, H. Stoll, A. J. Stone, R. Tarroni, T. Thorsteinsson and M. Wang, *MOLPRO, version 2012.1, a package of ab initio programs*, 2012, see http://www.molpro.net.

68 G. Karlström, R. Lindh, P. Å. Malmqvist, B. O. Roos, U. Ryde, V. Veryazov, P. O. Widmark, M. Cossi, B. Schimmelpfennig, P. Neogrady and L. Seijo, *Comput. Mater. Sci.*, 2003, **28**, 222–229.

69 F. Aquilante, L. De Vico, N. Ferré, G. Ghigo, P. Malmqvist, P. Neogrády, T. B. Pedersen, M. Pitoňák, M. Reiher, B. O. Roos, L. Serrano-Andrés, M. Urban, V. Veryazov and R. Lindh, *J. Comput. Chem.*, 2010, **31**, 224–247.

70 W. Weber, *PhD thesis*, University of Zürich, 1996.

71 W. Weber and W. Thiel, *Theor. Chem. Acc.*, 2000, **103**, 495–506.

72 A. Koslowski, M. E. Beck and W. Thiel, *J. Comput. Chem.*, 2003, **24**, 714–726.

73 W. Thiel, *MNDO99 program, version 6.1*, 2007, Max-Planck-Institut für Kohlenforschung, Mülheim, Germany, 2007.

74 D. R. Yarkony, *J. Chem. Phys.*, 2001, **114**, 2601–2613.

75 T. W. Keal, A. Koslowski and W. Thiel, *Theor. Chem. Acc.*, 2007, **118**, 837–844.

76 G. Granucci, M. Persico and A. Zoccante, *J. Chem. Phys.*, 2010, **133**, 134111–134119.

77 M. R. Silva-Junior and W. Thiel, *J. Chem. Theory Comput.*, 2010, **6**, 1546–1564.

78 M. Barbatti, A. J. A. Aquino, J. J. Szymczak, D. Nachtigallova, P. Hobza and H. Lischka, *Proc. Natl. Acad. Sci.*, 2010, **107**, 21453–21458.

79 D. Nachtigallova, T. Zeleny, M. Ruckenbauer, T. Müller, M. Barbatti, P. Hobza and H. Lischka, *J. Am. Chem. Soc.*, 2010, **132**, 8261–8263.

80 T. Zelený, M. Ruckenbauer, A. J. A. Aquino, T. Müller, F. Lankaš, T. Dršata, W. L. Hase, D. Nachtigallova and H. Lischka, *J. Am. Chem. Soc.*, 2012, **134**, 13662–13669.

81 H. L. Tao, B. G. Levine and T. J. Martinez, *J. Phys. Chem. A*, 2009, **113**, 13656–13662.

82 M. Richter, P. Marquetand, J. González-Vázquez, I. Sola and L. González, *J. Phys. Chem. Lett.*, 2012, **3**, 3090–3095.

83 L. Martínez-Fernández, I. Corral, G. Granucci and M. Persico, *Chem. Sci.*, 2014, **5**, 1336–1347.

84 G. L. Cui and W. Thiel, *J. Chem. Phys.*, 2014, **141**, 124101–124113.

85 G. L. Cui and W. Thiel, *Angew. Chem. Int. Ed.*, 2013, **52**, 433–436.

86 G. L. Cui, Z. G. Lan and W. Thiel, *J. Am. Chem. Soc.*, 2012, **134**, 1662–1672.

87 G. L. Cui and W. Thiel, *Phys. Chem. Chem. Phys.*, 2012, **14**, 12378–12384.

88 L. Spörkel, G. L. Cui, A. Koslowski and W. Thiel, *J. Phys. Chem. A*, 2013, **118**, 152–157.

89 L. Spörkel, G. L. Cui and W. Thiel, *J. Phys. Chem. A*, 2013, **117**, 4574–4583.

90 O. Weingart, Z. G. Lan, A. Koslowski and W. Thiel, *J. Phys. Chem. Lett.*, 2011, **2**, 1506–1509.

91 A. Kazaryan, Z. G. Lan, L. V. Schafer, W. Thiel and M. Filatov, *J. Chem. Theory. Comput.*, 2011, **7**, 2189–2199.

92 Y. Lu, Z. G. Lan and W. Thiel, *Angew. Chem. Int. Ed.*, 2011, **50**, 6864–6867.

93 E. Fabiano, T. W. Keal and W. Thiel, *Chem. Phys.*, 2008, **349**, 334–347.

94 J. B. Schönborn, A. Koslowski, W. Thiel and B. Hartke, *Phys. Chem. Chem. Phys.*, 2012, **14**, 12193–12201.

95 J. B. Schönborn and B. Hartke, *Phys. Chem. Chem. Phys.*, 2014, **16**, 2483–2490.

96 R. B. Gerber, D. Shemesh, M. E. Varner, J. Kalinowski and B. Hirshberg, *Phys. Chem. Chem. Phys.*, 2014, **16**, 9760–9775.

97 D. Shemesh, S. L. Blair, S. A. Nizkorodov and R. B. Gerber, *Phys. Chem. Chem. Phys.*, 2014, **16**, 23861–23868.

98 S.-H. Xia, B.-B. Xie, Q. Fang, G. Cui and W. Thiel, *Phys. Chem. Chem. Phys.*, 2015, **17**, 9687–9697.

99 W. Humphrey, A. Dalke and K. Schulten, *J. Mol. Graphics*, 1996, **14**, 33–38.